ТОМ 35 ОКТЯБРЬ—ДЕКАБРЬ, 1991 ВЫПУСК 2, 3

УДК 524.354.6—622

ON THE STUDY OF INTERNAL STRUCTURE OF SUPERDENSE CELESTIAL BODIES

G. T. TER-KAZARIAN

Received 2 april 1991

Accepted 10 may 1991

Different in principle from the contemporary standard black hole accretion models a new approach to the understanding of internal structure of highly compact stationary supermassive celestial bodies has been worked out. The equations of equilibrium configurations of baryonic protomatter (ECBP) have been discussed. In a particular case of ideal degenerated neutron gas in absence of the process of inner distortion of space and time, it has been shown that the suggested by the author theory leads to the same results as those obtained by Oppenheimer and Volkoff based on Einstein's theory. The numerical integration of equations of ECBP in the most simple case of equilibrium single-component configurations of degenerated ideal gas of neutrons in the presence of one-dimensional space-like inner distortion of space-time continuum is carried out. It has been shown that the stable stationary supermassive cores are formed in the central parts of considered configurations. As the models of active galactic nuclei (AGNs) one has considered only the configurations consisting of these cores surrounded by accretion disks. The fundamental difference from the standard black hole accretion models is the fact that the central cores are in stable equilibrium state with certain radial distributions of density and pressure and with a number of integral characteristics. The significant effect of metric singularity cut-off has been established, due to the action of which a singularity of metric ceases to be significant. The numerous integrations also have revealed an other fact of great importance of the presence of a rigorous restriction within the outlined theory on the upper limit of possible values of total masses of considered equilibrium configurations, which is to be $M \leqslant 3.5 \times 10^8 M_\odot$. In the last section one has proceeded to the direct modelling of concrete AGNs (for 61 sources), a whole point of which comes to the solving of an inverse problem. The results of all calculations which have been carried out in the present work are summarized in tables 1—5 and are represented by means of a few figures. At last one should emphasize the important fact of the existence of BL Lac objects OJ 287, 3C 66A and B2 1308+32, the observed timescale for flux variations of which are inconsistent with contemporary black hole accretion models. The case is quite different within the scope of the suggested theory. It seems that a decisive significance for these objects has the action of metric singularity cut-off effect. Due to it their observed sizes appeared to be less than the sizes of corresponding spheres of event horizon. This may serve as a further indication that suggested theory is preferable against the standard models.

1. *Introduction*. There is a sufficiently large number of observational data in astrophysics which proves the presence of highly compact supermassive formations existing in the stable stationary state for a long time compared to the age of the Universe. The important astrophysical phenomenon like the active galactic nuclei (AGNs) with super-Eddington luminosity is related to such objects. It is generally accepted to describe AGNs by means of standard black hole accretion models [2—5]. In standard scenario the central engine is a massive black hole into which a matter accretes through an accretion disk. According to conventional physics, the massive black holes must exist in these celestial bodies as well as in the nuclei of all galaxies that have ever experienced a violently active phase, just because of their more efficient power supply. A black hole has been formed as an almost inevitable endpoint of the gravitational collapse of a large fraction of total mass of supermassive configuration which has took place after the entire burning of the whole ammount of spared intrinsic energy. The standardized black hole is characterized by just two parameters — mass and spin — and is described by the Kerr metric. The black holes are being fueled steadily via the thick accretion disks. Such evolutionary processes of accretion onto massive black holes as the prime energy sources have immense emissive power. Due to it the idea that they can provide observed superhigh luminosity of AGNs becomes widely acknowledged among the astrophysicists.

The fact that accretion processes really take place in AGNs seems to be already established and proved for certain by lots of observations. Within respect to standard models one should note that such approach to understanding of physics of superdense equilibrium configurations, based on the main idea of black holes, suffers from some grave shortcomings. First among them—a fate of collapsing sphere, with respect to the proper coordinate system that is being used, remains indefinite. Due to such unbelievably extreme conditions when a theory breaks down inside the black hole where static observers cannot exist, because they are inexorably drawn into the central singularity, the possibility for calculation of corresponding integral characteristics of AGNs, particularly such as the total mass, radius etc., is absent. But the main deficiency is the fact that observed time-scales for flux variations of some objects are inconsistent with contemporary black hole accretion models. That is on the base of the diagram of the minimum variability time-scale against the bolometric luminosity for 60 sources it has been shown that few BL Lac objects—B2 1308+72, 3C 66A, OJ 287, AO 0235+16 and Quasars—3C 345, 3C 446, 3C 454.3, LB 9743 remained in forbidden zone (particularly the initial three of them)

[6, 7]. Therefore the creation of new viable theoretical constructions for the explanation of an abudant specter of observational data, especially for the understanding of physics of the considered above celestial bodies, is a problem of paramount importance.

An alternative approach to the understanding of internal structure of these objects is outlined by the author [8—10], who makes use of a basic assumption that supermassive stable cores exist in their central parts. Of course, it is impossible to obtain the solution of this problem within the scope of well established and generally accepted contemporary theoretical conceptions, because of fundamental difficulties encounter: 1. The presence of gravitational radius as the lowest limit for valid radius of any gravitating mass at hydrostatic equilibrium: 2. The problem of hydrostatic equilibrium of such configuration under the condition of high increase of its total mass.

Actually, General Relativity imposes a rigorous restriction on a possible upper limit of density. For example, a condensed matter of order of magnitude of galaxy mass should have radius $R < (9/8)\, R_g \simeq \simeq 0.01$ pc and density $\rho < 2 \cdot 10^{-6}\ gcm^{-3}$ (R_g is gravitational radius).

While super-increasing of total mass of configuration one undoubtly achieves (irrespective of the used theory) a critical turning point, beyond which the gravitational forces of compression become dominant (a stage of relativistic collapse). Moreover, it is enough to add from the outside a small amount of energy near-by the critical point in order to begin a process of irresistible infinite catastrophic compression of configuration under the pressure of grand forces. That is how the matter stands, as nothing can hold the collapse untill one shouldn't point out a concrete mechanism which can provide a proportional increase of internal pressure of gas with the rising in amount of mass of configuration (that is, with the increase of gravitational forces). Only due to validity of hydrostatic equilibrium a supermassive formation can really remain in a stable state for a long time.

Recently an opportunity has risen to overcome the mentioned above difficulties on the base of gravitational theory which is worked out in [1]. For the first time, the latter enables us to assume the quite new properties of space-time displayed in the region of small space-time intervals and to study the processes proceeding under such conditions. This fact apparently has decisive importance for more profound understanding of the physics of superdense matter.

At a superhigh density greater than a nucleus ($\rho > 2.85 \cdot 10^{14} \mathrm{gcm}^{-3}$, $N > 10^{39}\,\mathrm{cm}^{-3}$, to which the distances $\leqslant 0.4$ Fermy correspond) a space-time continuum is distorted [1]. Under this condition the quite new

phenomena are displaied. First among them — an acquisition of distorted energy-momentum and mass at rest of particle. A second — an asymptotic freedom of interaction of fields, which is carried out by means of the vector gauge fields. Due to the first each particle of gas undergoes the phase transition and, hence, goes off from the mass shell. Under such conditions law of conservation of energy-momentum in conventional form is substituded by a new one, that is the conservation law of distorted (generalized) energy-momentum of isolated system is found in distorted space-time continuum. Due to the second phenomenon the nuclear repulsive forces between baryons are damping down to zero with an increase of density of configuration.

New phase state of matter, which is found in distorted space-time continuum, will be called a protomatter. As one should be convinced later on, within the scope of the theory suggested below just the process of inner distortion of space-time provides the proportional rising of internal pressure of degenerated baryon gas with the increase of gravitational forces of compression. This process counteracts of the catastrophic collapse and a stable equilibrium remains valid even up to the limit of masses much greater than Solar mass.

The mentioned above phenomena are directly due to the global properties of space-time continuum, that is why they hold irrespective of the chosen model of configuration.

The present paper is dedicated to the study of the internal structure of supermassive compact celestial bodies and their modelling by means of numerical methods.

2. *The equations of equilibrium configurations of baryonic protomatter* (*ECBP*). For simplicity, we shall treat the spherical—symmetric configurations. The set of equations of ECBP, which determines the internal structure of such configurations (at „zero temperature"), involves the equations of fields of gravitation and inner distortion, the equations of hydrodynamic equilibrium and state of baryonic protomatter. In the case of the absence of transversal stresses and transference of masses in spherical-symmetric distribution of matter, which is found in distorted space $\underset{f}{P}(3)$, the energy-momentum tensor is given as follows:

$$T_1^1 = T_2^2 = T_3^3 = -P^f(r), \quad T_0^0 = \rho^f(r), \quad r \in \underset{f}{P}(3), \tag{2.1}$$

where $P^f(r)$ and $\rho^f(r)$ are the proper pressure and macroscopic density of energy of protomatter correspondingly (which are measured with respect to the proper frame of reference that is being used).

a) The equations of fields of gravitation $a_0(r_p)$ and inner distortion $\tilde{a}_{0\alpha}(r_p)$, $\bar{a}_\alpha(r_p)$ $(\alpha = 1, 2, 3)$ are written down

$$\Delta_r a_0 = -(1/2)\{g_{00}(\partial g^{00}/\partial a_0)\rho^f(r) - [g_{33}(\partial g^{33}/\partial a_0) + g_{11}(\partial g^{11}/\partial a_0) + g_{22}(\partial g^{22}/\partial a_0)]P^f(r)\}, \tag{2.2}$$

$$(\Delta_\rho - c^2 m_\alpha^2/h^2)\tilde{a}_{0\alpha} = -(1/2)\{g_{00}(\partial g^{00}/\partial \tilde{a}_{0\alpha})\rho^f(r) - [g_{33}(\partial g^{33}/\partial \tilde{a}_{0\alpha}) + g_{11}(\partial g^{11}/\partial \bar{a}_{0\alpha}) + g_{22}(\partial g^{22}/\partial \bar{a}_{0\alpha})]P^f(r)\}\theta(h/m_\alpha c - n^{-1/3}), \tag{2.3}$$

$$(\Delta_\rho - c^2 m_\alpha^2/h^2)\bar{a}_\alpha = -(1/2)\{g_{00}(\partial g^{00}/\partial \tilde{a}_\alpha)\rho^f(r) - [g_{33}(\partial g^{33}/\partial \tilde{a}_\alpha) + g_{11}(\partial g^{11}/\partial \bar{a}_\alpha) + g_{22}(\partial g^{22}/\partial \bar{a}_\alpha)]P^f(r)\}\theta(h/m_\alpha c - n^{-1/3}), \tag{2.4}$$

Here $g_{\mu\nu}$ is the metric tensor of curved and inner distorted continuum $\hat{g} : T_p \otimes T_p \to C^\infty(P_f(3) \oplus T_f(1))$, m_α is a mass at rest of fields $\bar{a}_{0\alpha}$ and $\tilde{a}_\alpha$, $r_p \in P(3)$, $P(3)$ is a three-dimensional plane space, n is an ordieary concentration of baryons, and a step function $\theta(t)$ is given

$$\theta(t) = \begin{cases} 1 & t \geqslant 0, \\ 0 & t < 0. \end{cases} \tag{2.5}$$

Diffeomorphism $r(r_p) : P(3) \oplus T(1) \to P_f(3) \oplus T_f(1)$ is defined by means of formula

$$r_p = r - R_g/4. \tag{2.6}$$

Compton length of fields $\tilde{a}_{0\alpha}$ and $\bar{a}_\alpha$ is less than or equal to 0.4 Fermi

$$h/m_\alpha c \leqslant 4 \times 10^{-14}\ \text{cm}. \tag{2.7}$$

b) The equation of hydrostatic equilibrium has a form

$$\partial P^f/\partial r + (\rho^f + p^f)F = 0, \tag{2.8}$$

where

$$F = g^{01}\partial g_{00}/2\partial r. \tag{2.9}$$

c) Due to the inner distortion of a continuum $P(3) \oplus T(1)$, each particle of gas undergoes the phase transition as follows:

$$\begin{aligned} &E_k \longrightarrow E_k^f, \\ &\vec{P}_k \longrightarrow \vec{P}_k^f, \\ &m_k \longrightarrow m_k^f. \end{aligned} \qquad \begin{aligned} &(E_k,\ \vec{P}_k,\ m_k) \sim P(3) \oplus T(1), \\ &(E_k^f,\ \vec{P}_k^f,\ m_k^f) \sim \underset{f}{P}(3) \oplus \underset{f}{T}(1), \end{aligned} \tag{2.10}$$

where E_k, $\vec{P}_k$, m_k are the energy, momentum and mass at rest of particle of k-th type.

It is true that the parameters of ordinary configurations of baryonic matter are sensitive to any change of equation of state. But it is a well established fact too that no change of this equation (if only one doesn't take into account the mentioned phenomenon of distortion of space-time) can lead to superlarge masses of configurations. Analogous to the standard method the state equation of baryonic protomatter has derived from a general principle of minimum of density of distorted energy of configuration and also by using of conservation laws of baryonic and electric charges. In the region of densities above nucleus the miscellaneous stable hyperons emerge just because of Pauli's principle. At the sufficiently high density, when all types of baryons are presented in a medium, one gets:

$$\rho^f = K_n^f \sum_k \delta_k^f (\operatorname{sh} t_k^f - t_k^f) + n^f U^f(n^f) + n_n^f m_n^f c^2, \tag{2.11}$$

$$P^f = (1/3) K_n^f \sum_k \delta_k^f (\operatorname{sh} t_k^f - 8 \operatorname{sh}(t_k^f/2) - 3t_k^f) + (n^f)^2 dU^f(n^f)/dn^f, \tag{2.12}$$

where

$$\begin{aligned} &t_k^f = 4 \operatorname{arsh}(P_k^f/m_k^f c), \quad K_n^f = (m_n^f)^4 c^5/32\pi^2\hbar^3, \\ &\delta_k^f = (m_k^f/m_n^f)^4, \qquad P_k = (3\pi^2)^{1/3} \hbar n_k^{1/3}, \\ &P_k^f = (3\pi^2)^{1/3} \hbar (n_k^f)^{1/3}. \end{aligned} \tag{2.13}$$

Here one makes summation over all baryons, m_n^f is distorted mass at rest of neutron, P_k^f is distorted Fermi momentum, n_k^f is distorted concentration of particles. To make use of proper formulae one can determine all t_k^f by means of corresponding parameter of neutron t_n^f. Therefore the problem can be reduced to determination of t_n^f as a function of radial distance. Actually the parameters t_k^f are functions of corresponding concentrations of particles, but in its turn some relations are

valid between the latters. One should note that a phase stratification of configuration of mixed baryonic gas also takes place in considered case of inner distortion of space-time. For instance one can readily show that the following relations present between distorted concentrations of baryons with the same electric charges

$$n_i^f = n_k^f [1 - (B_i^f / n_k^f)^{2/3}]^{3/2}, \tag{2.14}$$

where B_i^f are the threshold densities

$$B_i^f = (1/3\pi^2)(m_i^f c/h)^3 [1 - (m_k^f/m_i^f)^2]^{3/2}. \tag{2.15}$$

The relation (2.14) is valid for any selection of baryons.

The nuclear forces are transfered by means of quanta of Yang-Mill's vector gauge fields. Therefore according to [1] a nuclear potential energy U(n) for per baryon undergoes to the renormalization due to the distortion of continuum

$$U(n) \longrightarrow U^f(n^f, \tilde{\theta}). \tag{2.16}$$

where $\tilde{\theta}$ is the angle of inner distortion. One must distinguish the above mentioned phenomenon from the well known one predicted by Quantum Chromodynamics (QCD). According to it the strong interactions between the colour quarks which form the fundamental representation of group SU(3) are transfered by means of octet of glueons. Due to the scaling of strong interactions, that is the invariance under the transformations of renormalization group, a following law holds for a change of effective coupling constant equaling in lowest order to $g^2(\mu_0)$ and including a correction of $O(g^4(\mu_0))$

$$g^2(\mu) \simeq 8\pi^2 [(11/3) C_j - (4/3) C_f] \ln(\mu/\Lambda).$$

Here μ is an arbitrary scale in a mass measure, C_j is Dinkin's index of joint representation of group SU(3), Λ is a scale parameter of QCD

$$\ln \Lambda = \ln \mu_0 - 8\pi^2/g^2(\mu_0)[(11/3) C_j - (4/3) C_f].$$

For the group SU(3): $C_j = 3$, $C_f = 1/2$ for each Fermion, hence $C_f \to (1/2) n_f$, where n_f is a number of flavour ($n_f = 6$). Meanwhile if in considered model of configuration of protomatter one takes into account the scaling of strong interactions then the potential energy U(n) undergoes to the renormalization. Thereto, a phenomenon of inner distortion of space-time leads to secondary renormalization.

One should note that a baryonic protomatter fills the central part of equilibrium configuration. It is surrounded by the shell (where $\tilde{a}_{0\alpha} = \tilde{a}_\alpha = 0$) built up with three strata (npeA), (neA), (eA). Here n is a neutron, p is a proton, e is an electron and A is an atomic nucleus. The internal structure of equilibrium configuration is completely determined to make use of equations (2.2 — 2.16) if only the following functions are known

$$g_{\mu\nu} = g_{\mu\nu}(a_0, \tilde{a}_{0\alpha}, \tilde{a}_\alpha), \tag{2.17}$$

$$E_k^f = E_k^f(E_k, c\vec{P}_k, m_k c^2, \tilde{a}_{0\alpha}, \tilde{a}_\alpha), \tag{2.18}$$

$$\vec{P}_k^f = \vec{P}_k^f(\vec{P}_k, E_k/c, m_k c, \tilde{a}_{0\alpha}, \tilde{a}_\alpha), \tag{2.19}$$

$$m_k^f = m_k^f(m_k, E_k/c^2, \vec{P}_k/c, \tilde{a}_{0\alpha}, \tilde{a}_\alpha). \tag{2.20}$$

Therefore, it is necessary to determine just the functions (2.17 — 2.20) under the concrete physical conditions. This problem is solved in [1]. It has been shown that the shift of masses, the energy-momentum spectra of particles and due to it the shift of energy (density of mass) of gas as a whole upwards along the energy scale took place.

One should point out that the potentials a_0 and $(\tilde{a})$ presented in formulae (2.2 — 2.20) always remain positively defined. Otherwise they are devoid of physical sense.

At length it is necessary also to write down the line element form in the outside of the configuration ($r > r_b$, where r_b is a boundary of distribution of matter (see [1])

$$dS^2 = (1 - \varkappa a_0)^2 c^2 dt^2 - (1 + \varkappa a_0)^2 dr^2 - \\ - r^2(\sin^2\theta d\varphi^2 + d\theta^2), \tag{2.21}$$

where

$$\varkappa a_0 = R_g/2r, \quad \varkappa = 2\sqrt{\pi G}/c^2, \quad R_g = 2GM/c^2, \tag{2.22}$$

G is a gravitational constant.

On the base of state equation $\rho^f = \rho^f(P^f)$ the (2.8) is integrated, but a constant of integration is determined under the subsidiary condition to be imposed at the boundary of distribution. That is a continuity of metric through the passage at boundary ought to be valid

$$g_{00}(r_p) = (1 - R_g/2r_p^b)^2 \exp\left[\int_0^{P^f(r)} 2dP^f/(P^f + \rho^f)\right], \qquad (2.23)$$

where $r_p^b = r_p(r_b)$.

3. *The equations of equilibrium configurations of neutron protomatter (ECNP).* Thereafter we have to work out a detailed study of the problem in most simple case of equilibrium one-component configurations of ideal neutron gas in presence of one-dimensional space-like distortion of space-time continuum. Then to take into account the equations of ECBP (2.2 — 2.4) one readily gets in considered case the equations of spherical symmetric fields of gravitation $a_0(r_p)$ and space-like inner distortion $\tilde{a}(r_p)$ of plane continuum $P(3) \oplus T(1)$ ($r_p \in P(3)$, $\tilde{a}_{0\alpha} = \tilde{a}_1 = \tilde{a}_2 = 0$, $\tilde{a}_3 \equiv \tilde{a}(r_p)$, $\alpha = 1, 2, 3$)

$$\Delta_p a_0 = -(1/2)\{g_{00}(\partial g^{00}/\partial a_0)\rho^f(r) - [g_{33}(\partial g^{33}/\partial a_0) + g_{11}(\partial g^{11}/\partial a_0) + g_{22}(\partial g^{22}/\partial a_0)]P^f(r)\}, \qquad (3.1)$$

$$(\Delta_p - c^2 m_a^2/\hbar^2)\tilde{a} = -(1/2)\{g_{00}(\partial g^{00}/\partial \tilde{a})\rho^f(r) - [g_{33}(\partial g^{33}/\partial \tilde{a}) + g_{11}(\partial g^{11}/\partial \tilde{a}) + g_{22}(\partial g^{22}/\partial \tilde{a})]P^f(r)\} \times \times 6(\lambda_a - n^{-1/3}). \qquad (3.2)$$

Here $\Delta_p = \partial^2/\partial r_p^2$, $g_{\mu\nu}$ is a metric tensor of curved and inner distorted continuum $\underset{f}{P}(3) \oplus \underset{f}{T}(1)$ (see [1])

$$g_{00} = (1 - x_0)^2 + x^2,$$
$$g_{33} = -[(1 + x_0)^2 + x^2], \qquad (3.3)$$
$$g_{11} = -r^2, \quad g_{22} = -r^2 \sin^2\theta,$$

and

$$x_0 = \varkappa a_0, \quad x = \varkappa \tilde{a}.$$

A mass at rest of field $\tilde{a}$ is determined thereby Compton length $\lambda_a = \hbar/m_a c \simeq \lambda_0 = 0.4$ Fermi.

A function $\theta_i^f(t)$ is given by (2.5), a diffeomorphism $r(r_p)$: $P(3) \ominus T(1) \to \underset{f}{P}(3) \ominus \underset{f}{T}(1)$ is defined thereby (2.6). The equation of hydrostatic equilibrium has the form of (2.8, 2.9).

Due to the inner distortion of space-time continuum [1, 8 — 10] ($\tilde{\theta}^1 = \tilde{\theta}^2 = 0$, $\tilde{\theta}^3 \equiv \tilde{\theta}$, $\operatorname{tg}\tilde{\theta} = -x$) each neutron undergoes to the phase transition as follows

$$E_f = E,$$

$$P_{f\,1,2} = P_{1,2}\cos\tilde{\theta}, \quad P_{f\,3} = P_3 - m_n c \operatorname{tg}\tilde{\theta}, \tag{3.4}$$

$$m_n^f = [\,|(m_n - \operatorname{tg}\tilde{\theta}\cdot P_3/c)^2 + \sin^2\tilde{\theta}\cdot(P_1^2 + P_2^2)/c^2 - \operatorname{tg}^2\tilde{\theta}\cdot E^2/c^4\,|\,]^{1/2},$$

where E, $\vec{P}$, m_n are ordinary and E_f, $\vec{P}_f$, m_n^f — distorted energy, momentum and mass at rest of neutron.

According to the equations (2.11 — 2.13), the equation of state of degenerated ideal neutron protomatter has the form

$$\rho^f = m_n^f c^2 \chi(y_f)/\lambda_f^3, \quad P^f = m_n^f c^2 \varphi(y_f)/\lambda_f^3, \tag{3.5}$$

where

$$\chi(y_f) = (1/8\pi^2)\,[y_f(1+y_f^2)^{1/2}(1+2y_f^2) - \ln[y_f + (1+y_f^2)^{1/2}]],$$

$$\varphi(y_f) = (1/8\pi^2)[y_f(1+y_f^2)^{1/2}(2y_f^2/3 - 1) + \ln[y_f + (1+y_f^2)^{1/2}]], \tag{3.6}$$

$$m_n^f = m_n(|\eta|)^{1/3}, \quad \eta = 1 - x^2 - xy/\sqrt{3} - y^2x^4/6(1+x^2).$$

Thereat

$$y = P_F/m_n c = (3\pi^2)^{1/3}\lambda n^{1/3},$$

$$y_f = P_F^f/m_n^f c = (3\pi^2)^{1/3}\lambda_f (n^f)^{1/3}, \tag{3.7}$$

$$P_F^f = P_F\zeta^{1/2}, \quad \zeta = y[1 - 2x^2/(1+x^2)3] + 2xy/\sqrt{3} + x^2.$$

Here $\lambda = h/m_n c$, $\lambda_f = h/m_n^f c$. To simplify the problem in the formulae (3.6, 3.7) approximately are assumed $P_1 \simeq P_2 \simeq P_3 \simeq P/\sqrt{3} = |\vec{P}|/\sqrt{3}$, and in (3.7) a mean value of $\overline{P}/m_n c \simeq x_f/2$ is used. The appearance of modulus sign in (3.4 3.6) is due to the fact that in its absence a distorted mass of partical becomes imaginary for the values of $x \gg 1$. Such physical situation corresponds to the case when a distorted velocity of particle is greater than a local velocity of light, which depends on potential of field of inner distortion. One should point out that there is not any discrepancy because of the fact that in the metric theories usually instead of unobservable local coordinates are introdu-

ced the real standards of space and time intervals with respect to which the velocity of light always equals to its vacuum value. That is in the region of real values of m^f a parameter t^f is introduced in the integral expressions of P^f and p^f by usual way: $\mathrm{sh}\, t^f = P^f_p/m^f c$. But in the region of imaginary values of $m^{f'} = im^f$ the corresponding integrations are carried out in complex plane of distorted momenta of particles $\underset{f}{\vec{P}}$ along the imaginary axis. Hence one gets: $\mathrm{sh}\, t^{f'} = iP^f_p/m^f c = P^f_p/m^f c = \mathrm{sh}\, t^f$.

As to be mentioned early a neutron protomatter fills a central part of configuration and is surrounded by a shell (where $x = 0$) consisting of ordinary neutron gas.

4. *Neutron stars.* According to [1], the suggested theory of gravitation in the case of absence of inner distortion of space-time continuum and General Relativity are indiscernible from the point of view of post-Newtonian experiments. The essential differences arise only in strong fields. On the other hand it's well known that one among the most important merits of General Relativity is the prediction of existence of neutron stars, which are being observed afterwards. Then we come to the following question: what will be the results in the above mentioned theory in the region of strong gravitational fields which are typical for compact neutron stars? According to Oppenheimer and Volkoff's classical work the equilibrium configuration of ideal degenerated neutron gas has a possible maximum total mass $M \simeq 0.71 M_\odot$ ($M_\odot$ is Solar mass) and corresponding radius $R \simeq 9.5$ km. For the detailed study of this case one must put $x = 0$ in the equations of ECNP (hence the eq. (3.2) falls away). The ramaining equations are integrated by means of numerical methods leading off the center up to the surface of configuration, where internal pressure is equaled to zero. Each configuration is defined by the unique free parameter of central value of concentration of neutrons $n(0)$ or by equivalent to it a parameter of central density. One should note that it's necessary for the interior solution of gravitational potential $x_0^{\mathrm{int}}(r_p)$ to be continuously transformed to the exterior one $x_0^{\mathrm{ext}}(r_p)$

$$x_0^{\mathrm{int}}(R_p) = x_0^{\mathrm{ext}}(R_p), \tag{4.1}$$

where R_p is the radius of star in terms of plane space $P(3)$. According to (6) this relates to corresponding R ($R \in \underset{f}{P}(3)$) by means of formula

$$R_p = R - R_g/4. \tag{4.2}$$

Inasmuch as $x_0^{ext}(R_p) = R_g/2R_p$, then $x_0^{int}(R_p) = R_g/2R_p$. Now one introduces a dimensionless parameter of sewing

$$D = [x_0^{int}(R_p) - x_0^{ext}(R_p)]/x_0^{int}(R_p). \tag{4.3}$$

To solve the equation (24) one must choose two unknown constants in order to satisfy the subsidiary condition of sewing to be imposed at the boundary of configuration

$$D = 0. \tag{4.4}$$

The determination of these constants in its turn is entirely equivalent to definition of central value of gravitational potential $x_0(0)$, thereat the (4.4) holds. The latter is to be found by means of multiple repeated integrations.

The results of numerical integrations are summarized in table 1, where the coordinates of point of origin are presented in the third column, leading from which the integrations are carried out. The maximum values of total masses of configurations with different $x_0(0)$ are presented in the fourth column. One can see from table 1 that the possible maximum values of total masses of equilibrium configurations of ideal neutron plasma are equaled to $M/M_\odot = 0.717 \div 0.74$ and the corresponding radii $R = (8.5 \div 9.8)$ km. Hence suggested in [8—10] the theory, which is based on a new approach to the problem of gravitational interaction [1], almost leads to the same results obtained by Oppenheimer and Volkoff, based on Einstein's theory.

Table 1

THE PARAMETERS OF DEGENERATED NEUTRON STARS

$x_0(0)$	$n(0)(\mathrm{cm}^{-3})$	$r(0)$ (cm)	max $(M/M_\odot)$	R (km)
1	2	3	4	5
0.001	3.4143E+39	6.84E--04	2.595E—01	4.85025
0.01	3.4143E+39	6.84E—04	2.596E—01	4.93341
0.1	3.4143E+39	6.84E—04	2.505E—01	6.01669
0.5	7.7598E+40	1.37E—05	2.559E—01	4.38965
0.7	3.4143E+41	6.84E—04	2.595E—01	5.05557
0.78	6.2047E+41	1.37E—05	2.464E—01	6.24531
0.9	9.3117E+42	4.10E+01	2.599E—01	5.00751
0.95	7.5735E+43	1.37E—05	2.597E—01	5.00117

Table 1 (Continued)

1	2	3	4	5
0.999	3.1039E+49	1.37E−05	1.886E - 01	2.53866
0.9999	9.2838E+51	1.37E−05	2.596E−01	4.98599
1	9.3117E+28	6.84E−04	2.593E−01	4.81568
1.5	9.3117E+28	6.84E−04	2.491E−01	4.00817
1.5	1.5519E+40	6.84E−04	1.605E−01	2.10943
2	9.3117E+28	6.84E−04	1.936E−01	2.62276
2	3.1039E+38	6.84E−04	2.531E−01	4.20581
5	9.3117E+28	6.84E−04	2.856E−01	4.71822
5	1.7071E+37	6.84E−04	3.912E−02	6.05704
7	9.3117E+28	6.84E−04	1.341E−02	2.61665
7	9.3117E+38	6.84E−04	1.769E−02	3.24473
10	3.1039E+29	6.84E−04	7.466E−03	1.66587
10	1.2416E+37	6.84E−04	1.123E−02	2.28268
30	9.3117E+28	6.84E−04	6.092E−04	2.40116
30	2.1727E+35	6.84E−04	1.357E−03	4.56641E−02
30	3.1039E+40	6.84E−04	2.676E−04	1.26811E−02
45	3.1039E+29	6.84E−04	2.220E−01	5.25529
45	9.3117E+30	6.84E−04	2.264E−01	5.37482
45	3.1039E+32	6.84E−04	2.653E−01	20.14247
50	3.1039E+31	6.84E−04	7.173E−01	9.83287
50	2.7929E+34	6.84E−04	7.409E−01	8.51466
50	4.6559E+34	6.84E−04	7.251E−01	9.49235
65	1.5519E+31	6.84E−04	6.885E−01	7.02449
65	2.1727E+31	6.84E−04	5.528E−01	7.14511
65	1.5519E+34	6.84E−04	5.919E−01	6.68971
65	3.1039E+32	6.84E−04	5.438E−01	7.11628
73	3.1039E+31	6.84E−04	2.442E−03	1.08482
100	3.1039E+35	6.84E−04	1.162E−04	6.39424
1466.41	3.1039E+37	6.84E−04	4.966E−01	6.71726
1466.7	3.0635E+29	6.84E−04	4.616E−01	7.54962
1466.7	3.1039E+37	6.84E−04	3.782E−01	7.67247
1467	3.1039E+37	6.84E−04	2.337E−01	6.41773

Below one presents a figure 1 related to neutron stars with the central value $x_0(0) = 50$. Among them the maximum values of total masses $M/M_\odot = 0.717 \div 0.74$, are achieved for the configurations with the central concentrations $n(0) = (3.1 \cdot 10^{31} \div 2.74 \cdot 10^{34})\ \mathrm{cm}^{-3}$, thereat $r(0) = 6.84 \cdot 10^{-4}$ cm. Here

$$M = (4\pi/c^2)\int_0^R \rho' r^2 dr,$$

$$M_1 = (4\pi/c^2)\int_V \rho' dV, \tag{4.5}$$

$$M_0 = Nm_n = \int_V m_n n dV,$$

and

$$dV = 4\pi(-g_{33})^{1/2} r^2 dr$$

is an element of volume, N is a total number of neutrons. One should note that the macroscopic energy apart from the energy at rest includes also the energy of the motion of neutrons and the energy of interaction of particles in per 1 cm^{-3}. That is why the total mass M of the star is not equal to the sum M_1 of the masses of volume elements. Moreover, due to the inequality $(-g_{33})^{1/2} > 1$ one has $M < M_1$. The other mass M_0 is calculated without taking into account a binding energy of gravitational interaction between the neutrons.

As one can see through fig. 1 the stable configurations correspond to the curve length on which a criterion $dM/d\rho(0) > 0$ for identifying stability is valid. They represent the neutron star models characterized with the central values of density within the limits as follows: $4.32 \times \times 10^{-10} \leqslant \rho(0)/\rho_0 \leqslant 1.44 \cdot 10^{-7}$; $7.2 \cdot 10^{-5} \leqslant \rho(0)/\rho_0 \leqslant 2.16 \cdot 10^{-4}$ and with radius $R \simeq (3.57 + 9.8)$ km.

5. *The models of AGNs.* In this section we are going to carry out the numerical integration of equations of ECNP already in the presence of the process of inner distortion of space-time continuum. As it was mentioned earlier displayed under this conditions new phenomena directly relate to the global properties of space-time continuum at small space-time intervals. Hence they hold irrespectively to the choice of the model of configuration. Due to it, and as one should see later on, the further modifications of models in sense of change of form of state equation to the other one of real baryonic gas cannot lead to the perceptible corrections. That is why we have carried out our calculations for the most simple case of equilibrium one-component configurations of degenerated ideal gas of neutrons in presence of one-dimensional space-like inner distortion of space-time continuum. Right now each configuration is defined by two parameters of central values

of concentration of neutrons $n(0)$ and of field $^{r}x(0)$ of pure inner distortion of continuum. Thereat a central value of gravitational potential $x_0(0)$ is to be found by means of multiple integrations through with the subsidiary sewing condition (4.4) of interior and exterior solutions has been imposed at a boundary of configuration.

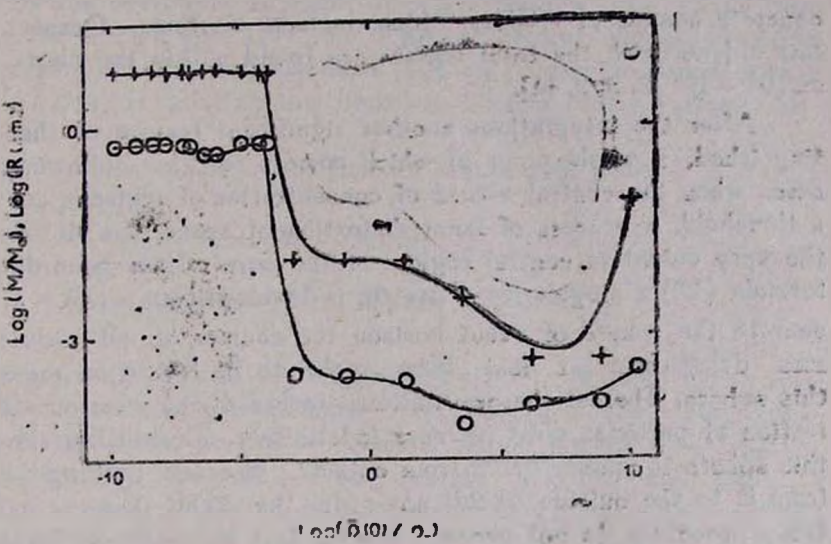

Fig. 1. Schematic diagram showing the mass and radius versus central density of the neutron star $\rho_0 = 2.8 \times 10^{14}$ (g. sm^{-3}), O — Log ($M / M_{\odot}$), + — Log (R (km)).

After the integrations cleared up the following scenario. In the central part of superdense core of neutron protomatter due to the inner distortion of space-time continuum the pressure increases proportionally to the rising in an amount of total mass (that is to the upgrowth of gravitational forces of compression). This process counteracts to coms pression of central part of core. Hence the stable equilibrium remain-valid in its outward layers too, even up to limit of masses much greater than Solar mass. The radius of supermassive stable core turns out approximately to be equaled $R \simeq R_g/4$, hence it has been wholly found within the sphere of even horizon with the radius $R_n = (3/4)\, R_g$ (see formulae (2.6), (2.22), (3.3), (4.2)). These cores can be observed only in the presence of accreting matter in their immediate vicinities. That is why from now on we shall consider only the configurations consisting of the above mentioned stable stationary supermassive central cores

surrounded by accretion disks. The main difference from the standard black hole accretion models is the fact that the central cores are in stable equilibrium state with the certain number of radial distributions of density, pressure, etc and with the other integral characteristics such as the masses M, M_1, M_0, radius R_*, total number of baryons N, gravitational packing coefficients and so on.

Versus the parameters of central cores, such configurations present concrete models of AGNs, which include Seyferts, Quasars and BL Lac objects with the total masses are found within the limits $M/M_\odot \simeq \simeq 10^2 \div 10^8$ [2, 3, 5, 11].

After the integrations another significant feature of theory is distinguished, a whole point of which comes to the following. In those cases when the central values of concentration of neutrons are less than a threshold, a process of inner distortion of space-time is absent from the very outset in central region of the core. Then according to the formula (3.3) a singularity of metric is developed at $x_0(r_*^0) = 1$. Drawing near to the sphere of event horizon the courses of all physical processes delay and at last they ought to be frozen on the surface of this sphere. Thereat the gravitational forces of compression and concentration of particles must increase indefinitely. Eventually, the inside of this sphere is unobservable from outside, because nothing can escape from it to the outside world, not even the light. But actually all of these processes do not proceed too far just because, during an approaching to the surface of sphere, a concentration of neutrons at last achieves to threshold value and a counteracted mechanism engages. That is under such conditions a field of inner distortion of space-time continuum is switched on, the singularity of metric disappears and the inverse process of sharp decrease of concentration as well as of gravitational forces begins. The further integration along the radial direction is continuing in its usual way after a passage through a point of singularity. Thus the metric singularity cut-off process presents. We call it the metric singularity cut-off effect. As a matter of fact under such conditions a singularity of metric ceases to be significant after all. This effect can be especially decisive for those objects to which the accreting matter has steadily filled a whole inside of event horizon sphere in due course has formed a thick shell. The concentration of baryons in shell by increasing can at last achieve threshold value and afterwards the effect of metric singularity cut-off will act. Under such extreme conditions the event horizon vanishes and the particles and light can already escape from the object to the outside wold. A black hole is dead. In those special cases one can observe

the supermassive celestial bodies with the sizes turned out to be less than the sizes of corresponding event horizon spheres. As astrophysical observations have confirmed the cosmic objects of such kind really exist n Nature, to which we should turn later on.

The results of numerical integrations are summarized in the Tables 2 and 3. As before, in table 2 n (0) is the central concentration of neutrons, $r(0)$ is the coordinate of point of origin leading from which the integrations are carried out, $\rho(0)$ and $P(0)$ are central values of density and pressure. D ts a dimensionless sewing parameter which is required to be $|D| \ll 1$ violating this limit equilibrium configurations cannot exist.

The gravitational packing coefficients are written down

$$A1 = \Delta_1 M/M = (M_1 - M)/M, \qquad A2 = \Delta_2 M/M_0 = (M_0 - M)/M_0 \tag{5.1}$$

where the masses M, M_1 and M_0 are given by (4.5). A coefficient A1 characterizes the ratio of gravitational energy against the total one, but A2 shows the whole portion of released energy during the formation of configuration. From table 3 one can see that the possible values of total masses of stable cores in terms of Solar mass are within the limits $M/M_\odot \simeq 10^3 \div 10^8$.

By means of these calculations we have been able to reveal another fact of great importance, which is the presence in outlined theory the rigorous restriction on the upper limit of possible values of total masses of considered configurations. This limit has to be $M \leqslant 3.5 \times \times 10^8 M_\odot$. The equilibrium configurations with the masses greater than this value cannot exist because of strong violation of subsidiary condition (4.4).

The Table data are rather lame to clear up completely the whole relations between the integral characteristics. Just because of it one fills a want with new calculations and corresponding to them figures for the concrete equilibrium configurations characterized by, e. g. the central values of potentials $x_0(0) = 500$ and $x(0) = 33.7$. After the calculations one readily obtains that their total masses are found within the limits $M/M_\odot = 1.068 \times 10^7 \div 3.925 \times 10^7$, and radii are reached up to $R = (7.912 \times 10^5 \div 2.901 \times 10^7)$ km. The all successes of these calculations can be seen from the diagrams 2 and 3.

On these diagrams the masses M, M_1, M_0 are plotted against the central density and pressure. As one can specify the stable configura-

Table 2

THE PARAMETERS OF CONFIGURATIONS OF DEGENERATED NEUTRON PROTOMATTER

No	$x_0(0)$	$x(0)$	$n(0)$ (cm^{-3})	$r(0)$ (cm)	$\rho(0)/\rho_0$	$P(0)/P_0$	D
1	2	3	4	5	6	7	8
1	2	0.1	4.6559E+52	1.37E−05	2.946E+18	2.065E+23	−4.13E−02
2	5	10	3.1039E+53	6.84E−04	3.974E+19	1.360E+21	5.93E−02
3	5	10	3.1039E+57	1.37E−05	8.717E+24	2.978E+26	1.65E−02
4	7	13	3.1039E+40	6.84E−04	7.341E+05	6.226E+08	−4.84E−02
5	7	13	3.1039E+43	6.84E−04	2.196E+07	1.881E+09	−8.00E−02
6	8	17	3.1039E+40	6.84E−04	2.022E+06	1.651E+09	3.46E−02
7	8	16	3.1039E+40	6.84E−04	1.607E+06	1.322E+09	−1.75E−02
8	8	16	3.1039E+44	6.84E−04	2.687E+08	9.324E+09	−2.23E−03
9	8	16	3.1039E+49	6.84E−04	3.012E+14	4.039E+15	−1.11E−03
10	10	19	3.1039E+40	6.84E−04	3.091E+06	2.491E+09	−8.57E−03
11	10	19	3.1039E+43	6.84E−04	6.128E+07	3.792E+09	4.14E−03
12	10	19	3.1039E+49	6.84E−04	3.591E+14	3.345E+15	2.34E−02
13	10	17	3.1039E+55	6.84E−04	3.072E+22	3.608E+23	3.78E−02
14	10	19	3.1039E+57	1.37E−05	1.621E+25	1.486E+26	−2.37E−02
15	10	17	3.1039E+57	2.74E−05	1.428E+25	1.643E+26	−7.84E−02
16	20	24	3.1039E+40	6.84E−04	7.583E+06	5.969E+09	−8.14E−03
17	20	24	3.1039E+43	6.84E−04	1.214E+08	6.366E+12	5.41E−02
18	20	24	3.1039E+47	1.37E−05	1.217E+12	8.966E+12	8.90E−02
19	20	24	2.0780E+57	1.37E−05	5.142E+25	3.283E+26	1.43E−02
20	50	27.7	3.1039E+43	6.84E−04	1.882E+03	9.023E+12	6.93E−02
21	50	27.7	3.1039E+41	6.84E−04	2.202E+07	8.999E+11	1.19E−03

Table 2 (Continued)

1	2	3	4	5	6	7	8
22	50	27.7	3.1039E+40	6.84E−04	1.320E+07	1.027E+12	−5.93E−02
23	50	27.7	3.1039E+57	1.37E−05	2.352E+25	7.729E+28	−7.77E−02
24	100	31.1	3.1039E+40	6.84E−04	2.044E+07	1.577E+10	−1.01E−02
25	100	31.1	3.1039E+58	1.37E−05	5.667E+26	1.579E+27	6.39E−02
26	100	31.1	3.1039E+57	1.37E−05	2.629E+25	1.177E+26	−7.35E−02
27	200	32.04	3.1039E+48	6.84E−04	3.161E+13	1.162E+14	−6.40E−03
28	200	32.04	3.1036E+42	6.84E−04	9.011E+07	1.245E+10	5.89E−04
29	200	32.04	3.1039E+45	6.84E−04	1.061E+10	8.681E+10	−5.97E−02
30	200	32.1	3.1039E+40	6.84E−04	2.341E+07	1.801E+10	−8.95E−01
31	500	33.7	3.1039E+51	6.84E−04	2.855E+17	9.555E+17	3.06E−01
32	500	33.7	9.3117E+52	6.84E−04	2.628E+19	8.825E+22	8.27E−02
33	500	33.7	3.1039E+53	6.84E−04	1.306E+20	2.502E+20	1.18E−01
34	500	33.7	5.8974E+53	6.84E−04	3.072E+20	2.848E+23	2.31E−04
35	500	33.7	3.0480E+45	6.84E−04	1.161E+10	8.749E+10	−1.29E−01
36	500	33.7	3.0420E+45	6.84E−04	1.159E+10	8.697E+10	−1.55E−01
37	500	33.7	2.1727E+52	6.84E−04	8.114E+19	3.473E+23	−1.78E−01
38	500	33.7	3.0729E+45	6.84E−04	1.169E+10	8.741E+10	−3.07E−01
39	500	33.7	2.2659E+50	6.84E−04	1.880E+17	5.144E+17	−2.25E−01
40	1000	34.4	5.3104E+46	6.84E−04	8.447E+11	4.586E+12	2.19E−01
41	1000	34.4	1.9626E+57	6.84E−04	4.392E+07	2.065E+10	−5.76E−01
42	1000	34.4	9.3117E+46	6.84E−04	4.632E+11	1.329E+12	−8.41E−01
43	2000	35	9.0323E+57	1.37E−05	1.233E+26	7.711E+25	−5.52E−01
44	2000	35	9.0013E+57	1.37E−05	1.228E+26	7.676E+25	−7.39E−01
45	2000	34.9	9.6221E+46	6.84E−04	6.356E+11	5.851E+11	−6.52E−01

Table 3

THE INTEGRAL PARAMETERS OF CONFIGURATIONS OF DEGENERATED NEUTRON PROTOMATTER

No	$M/M_\odot$	R (km)	R_g (km)	N/N_0	$A1$	$A2$
1	2	3	4	5	6	7
1	470.525	415.50	1389.76	4365.43	8.038	0.872
2	602.209	539.19	1778.70	6598.48	8.978	0.891
3	688.803	607.58	2034.47	7826.27	9.345	0.895
4	953.449	820.15	2816.13	12085.24	10.448	0.906
5	1255.496	1062.69	3708.27	17647.61	11.584	0·915
6	1521.484	1291.65	4493.89	24101.96	12.951	0.925
7	1543.812	1302.73	4559.85	24146.01	12.826	0.924
8	1877.074	1572.15	5544.18	31993.56	13.971	0.930
9	2057.065	1716.07	6075.81	36436.66	14.523	0.933
10	2964.565	2433.78	8756.22	60957.40	16.896	0.942
11	3354.432	2743.03	9907.74	72982.54	17.883	0.945
12	3609.924	2947.98	10662.37	81490.82	18.554	0.947
13	3938.167	3209.89	11631.88	92782.27	19.368	0.949
14	3983.312	3230.62	11765.22	92323.76	19.085	0.949
15	4323.943	3484.47	12771.32	101650.80	19.399	0.949
16	17354.530	13503.93	51258.82	758834.70	36.316	0.973
17	18119.330	14116.77	53517.77	824275.00	37.771	0.974
18	18295.450	14270.83	54037.96	847146.30	38.436	0.974
19	20576.610	15966.11	60775.64	975139.00	39.388	0.975
20	146518.200	110638.50	432760.20	1.695E+07	96.854	0.989
21	149949.000	113064.10	442893.50	1.699E+07	94.903	0.989

Table 3 (Continued)

1	2	3	4	5	6	7
22	151421.900	114066.60	447244.10	1.695E+07	98.744	0.989
23	175548.700	132051.20	518505.60	2.092E+07	99.836	0.990
24	678835.100	506574.30	2005026.00	1.530E+08	189.311	0.995
25	717635.100	535550.40	2119627.00	1.710E+08	200.150	0.995
26	781953.100	583054.50	2309599.00	1.859E+08	199.696	0.995
27	2744805.000	2038073.00	8107134.00	1.289E+09	394.897	0.997
28	3026450.000	2246691.00	8939006.00	1.393E+09	387.148	0.997
29	3204730.000	2378150.00	9465580.00	1.496E+09	392.703	0.997
30	5204097.000	3853400.00	1.537E+07	2.346E+09	379.565	0.997
31	1.068E+07	7912430.00	3.156E+07	1.257E+10	990.978	0.999
32	1.411E+07	1.045E+07	4.168E+07	1.664E+10	993.228	0.999
33	1.504E+07	1.113E+07	4.443E+07	1.775E+10	993.862	0.999
34	1.704E+07	1.261E+07	5.034E+07	2.014E+10	994.368	0.999
35	1.927E+07	1.426E+07	5.691E+07	2.247E+10	981.988	0.099
36	1.971E+07	1.458E+07	5.822E+07	2.298E+10	982.006	0.999
37	2.226E+07	1.646E+07	6.575E+07	2.627E+10	993.779	0.999
38	2.471E+07	1.827E+07	7.297E+07	2.881E+10	982.001	0.999
39	2.565E+07	1.897E+07	7.575E+07	3.019E+10	991.249	0.999
40	4.003E+07	2.959E+07	1.182E+08	9.356E+10	1969.103	0.999
41	8.331E+07	6.156E+07	2.461E+08	1.893E+11	1915.195	0.999
42	1.285E+08	9.497E+07	3.797E+08	3.005E+11	1969.400	0.999
43	2.715E+08	2.005E+08	8.018E+08	1.289E+12	3981.614	0.999
44	3.310E+08	2.445E+08	9.778E+08	1.564E+12	3981.816	0.999
45	3.469E+08	2.563E+08	1.025E+09	1.621E+12	3937.056	0.999

tions represent the models of AGNs characterizing by the central densities and pressures respectively as follows:

$$1.159\cdot10^{10}\leqslant\rho(0)/\rho_0\leqslant1.81\cdot10^{10},\ 5.425\cdot10^{14}\leqslant\rho(0)/\rho_0\leqslant5.786\cdot10^{16},$$
$$2.855\cdot10^{17}\leqslant\rho(0)\rho_0\leqslant2.422\cdot10^{18},\ 2.628\cdot10^{19}\leqslant\rho(0)/\rho_0\leqslant1.052\cdot10^{20},$$
$$1.306\cdot10^{20}\leqslant\rho(0)/\rho_0\leqslant2.242\cdot10^{20},\ 3.072\cdot10^{20}\leqslant\rho(0)/\rho_0\leqslant3.267\cdot10^{20},$$

and

$$8.697\cdot10^{10}\leqslant P(0)/P_0\leqslant9.151\cdot10^{10},\ 2.259\cdot10^{19}\leqslant P(0)/P_0\leqslant1.239\cdot10^{20},$$
$$8.825\cdot10^{22}\leqslant P(0)/P_0\leqslant1.161\cdot10^{23},\ 2.848\cdot10^{23}\leqslant P(0)/P_0\leqslant6.898\cdot10^{23}.$$

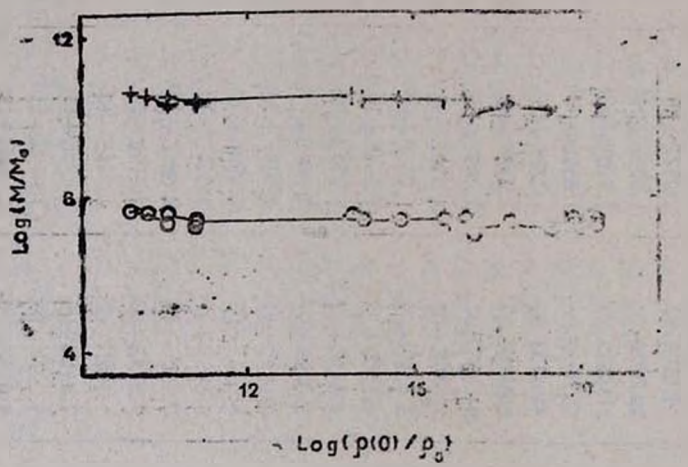

Fig. 2. Schematic diagram showing the masses M, M_0, M_1 versus central density of active galactic nucleus $\rho_0 = 2.8\times10^{14}$ (g. cm^{-3}), O — Log $(M/M_\odot)$, + — Log $(M_1/M_\odot)$, ÷ — Log$(M_0/M_\odot)$.

One must emphasize the fact that unlike to previous case of neutron stars, the weak dependence of integral characteristics over the central values of density and pressure is presented here. In its turn, it clearly indicates that the masses M, M_1, M_0 and other characteristics of AGNs will remain almost indifferent to any possible further change of the form of state equation to the other one of real barionic gas above a „neutron drip" ($\rho\geqslant4.3\cdot10^{11}$ g cm^{-3}) [12]. By the latter we mean to make use of the equations, e. g., such as the Harrison-Wheeller [13] or Baym-Bethe-Pethic [14] equations etc., or even the equation of the most exotic state of superdense nuclear matter, when the rearrangement of hadronic string connections or „flip-flop" takes place [15],

due to it the hadrons melt down and nuclear matter turns into quark matter.

That is, in the considered case all the dominant and signifiend processes actually realate directly to the global properties of space-time continuum at small intervals. As a matter of fact the modifications of the models in the above mentioned sense can not lead to any perceptible corrections.

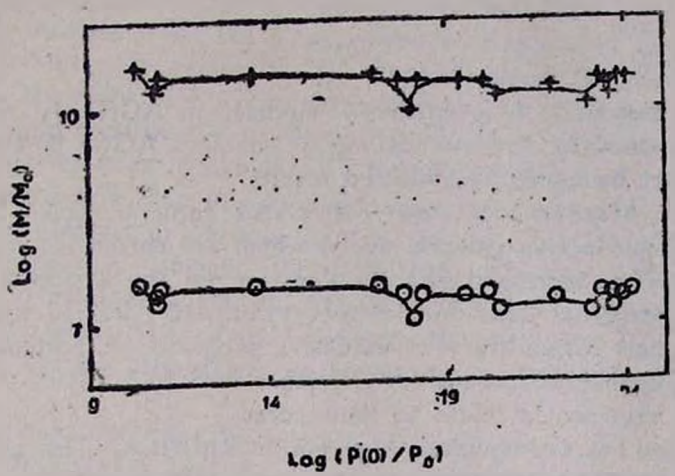

Fig. 3. Schematic diagram showing the masses M, M_0, M_1 versus central pressure of active galactic nucleus, $P_0 = 10^{33}$ (erg. cm^{-3}), O—Log $(M/M_\odot)$, + —Log $(M_1/M_\odot)$, ÷ —Log $(M_0/M_\odot)$.

According to the physics of internal structure of considered objects it is obvious that for stable, highly compact, supermassive configurations it must hold $\Delta_2 M > 0$, otherwise they have been unstable. In the considered case one has for the gravitational packing coefficient $A2 = 0.9989 > 0$.

The comparison of these calculations with the results of the previous section of the neutron stars has cleary shown that in the case of AGNs the process of pure inner distortion of space-time continuum actually led to the sharp increase of pressure of degenerated baryonic gas up to few orders of magnitude. This process counteracts to the collapse of central core. Meanwhile, the sound velocity has remained less than the velocity of light in the case of AGNs as well as it has been in the case of neutron stars. Actually, by the formulae (3.5 — 3.7) one can readily obtain

$$p^f \simeq p_N x^4$$

$$P^f \simeq P_N x^4,$$

for the large values of $x \gg 1$. Here ρ_N and P_N are correspondingly the density and pressure of the ordinary neutron star. Thus, in the central domain of the considered configurations one has

$$v^f = (dP^f/d\rho^f)^{1/2} \simeq (P^f/\rho^f)^{1/2} \simeq$$
$$\simeq (P_N/\rho_N)^{1/2} \simeq v \leqslant c,$$

for the velocity of sound.

Hence the study of preliminary models of AGNs is completed. We shall proceed to direct modelling of concrete AGNs in the section after the next by using the obtained results.

5. *Some observational data from active galactic nuclei.* The number of cataloged active galactic nuclei which are currently available in the literature has increased steadily almost over the last twenty years. Much of increase has been due to surveys of well—defined samples for polarization and variability. The extensive program of systematic multiwave length observations of AGNs must lead to a better understanding of the environment close to their cores.

AGNs are the sources of immense power of radiation. The astrophysical data across the whole spectrum of radiation define the minimum variability time-scale and bolometric luminosity, and also clear up the geometrical characteristics of their emission. Most of AGNs exibit short term intensity variations which are consistent with the existence of a highly compact central engine. In some cases the time-scales of the flux variations indicate that the conditions in the immediate vicinity of the emitting region are such that the Eddington luminosity limit for isotropic emission is violated. The flux variations impose direct restrictions on the theoretical models for AGNs [16] as well as on the possible accretion disk configurations [17]. In the case of a black hole model the minimum time-scale for flux variations $\Delta t_{\min}$ is equal or greater than the light travel time across the Schwarzschild radius of the black hole. Therein the observed luminosity and variability time-scale should obey the following relation [16]: $\log L \leqslant 43.1 + \log \Delta t_{\min}$. In [17] is considered the possibility of asymmetric emission model geometries which incorporate beaming of the radiation and obtained the corrected form: $\log L' \leqslant 43.3 + \log \Delta t_{\min}$. In [6, 7] the analysis of the variability time-scale-bolometric luminosity relation for 60 sources (Seyferts, Quasars and BL Lac objects) is presented. The estimates of $\Delta t_{\min}$ rely mostly on infrared-optical (both photometry and polarimetry) and x-ray obser-

vations. The detection of polarization depends not only on the precision of the polarimeter, but also on the luminosity of the AGNs. There are some difficulties, just because at low redshifts, starlight from the host galaxy can dilute the nuclear polarization. One must note that the selection effects depend on the exact sequence of the observations. Both values of Δt_{min} and L_{bol} have been corrected to their intrinsic values at the source, assuming Friedman cosmology with $q_0 = 1$ and $H_0 = 50$ kms^{-1} Mpc^{-1}. One should point out that the estimated values of L_{bol} must be regarded as lower limits on the true bolometric luminosities of the sources, while the Δt_{min} values may represent upper limits on the variability time-scales. In [7] a dependence of the number of sources upon the ratio of L/L_E (in units of classical Eddington value L_E) for each group clasification is plotted. It has been shown that while Seyfert Galaxies have luminosities within Eddington limit, the Quasars and BL Lac objects tend to approach and exceed this limit. On the basis of the diagram of $\log \Delta t_{min}$ against the $\log L_{bol}$ it is obtained that few objects (BL Lac objects—B2 1308 + 72, 3C 66A, OJ 287, AO 0235 + 16, Quasars—3C 345, 3C 446, 3C 454.3, LB 9743) are found in the forbidden zone. That is the observed time-scales for flux variations for this objects are inconsistent with contemporary black hole accretion models.

One should note that the relation of mass against the luminosity of sources in the case of isotropic emission is given by means of formula

$$M_s = 7.69 \times 10^{-47} L \text{ erg}^{-1} s, \tag{5.2}$$

which is obtained under the condition of balance between gravitation and radiation pressure. Here $M_n = M/10^n M_\odot$ is denoted. Now we turn to the case of anisotropic emission. That is one admits the possibility of asymmetric geometry of emission. Then from the formula (5.2) if one takes into account the beaming of radiation, due to it the additional coefficient $\log (L'/L) = 1.2$ appears, one gets

$$M_s = 4.85 \cdot 10^{-48} L \text{ erg}^{-1} s. \tag{5.3}$$

One should note that in AGNs the density of matter is much greater than radiation density, that is $M \gg 4RL/3c^3$, or $M_n \gg 2.51 \cdot 10^{-65} 10^{-n} RL \cdot \text{scm}^{-1} \text{erg}^{-1}$. For instance, if $n = 8$, $R_{max} = 10^{15}$ cm, one has $M_s \gg 2.51 \cdot 10^{-58} L$ erg^{-1} s.

6. *The modelling of AGNs.* According to the results of the fourth section one has been convinced in the correctness of the drawn before

statement that further modifications of considered models in the sense of change of the form of state equation to the other one of real baryonic gas can not actually lead to perceptible corrections. This enables us to procced to direct modelling of concrete AGNs, the main idea of which comes to the following. Based on the observational data first of all one defines the total mass M of concrete object by means of formula (5.3). Afterwards one solves the inverse problem. That is, thereby reiterated integrations of the equations of ECNP one has determined those required central values of concentration $n(0)$ and field of inner distortion of space-time continuum $x(0)$, for which the calculated total mass of configuration exactly equals to the same M. After the integrations one also has the whole set of basic integral characteristics.

All the results are presented in the Tables 4, 5. In Table 4 the name of object is given in the first column, but the type and waveband of variability—accordingly in the second and third columns, $r(0)$ is the coordinate of the centre, $\rho(0)$ and $P(0)$ are central values of density and pressure as denoted before. In the table 5 one has R_n as a radius of central stable stationary supermassive core, R_g its gravitational radius, $DR = R - (3/4)R_g$ (where $R = c\Delta t_{min}$) is the thickness of the accretion disk. As we have pointed out formerly the mass defect of the considered stable objects must be $\Delta_2 M = M_0 - M > 0$, or $A2 > 0$.

The fact of great importance of existence in Nature of the exotic stationary objects such as the BL Lac objects — OJ 287, 3C 66A and B2 1308 + 32 should be noted, which has clearly shown the fundamental difference between two approaches to the understanding of internal structure of highly compact supermassive celestial bodies. We mean the very difference between the outlined here theory and the standard black hole accretion models. Actually, within the scope of the latter one rule holds rigorously, according to which the celestial body with a size is less or equaled to the size of the corresponding sphere of event horizon cannot be observed by a distant observer. Meanwhile in spite of the auxiliary assumption of asymmetric emission geometry, nevertheless the above mentioned sources are found in a forbidden zone on the diagram of $\log \Delta t_{min} - \log L_{bol}$ [6].

The case is quite different within the scope of our approach. The discussed discrepancy can be resolved as follows. It seems that for these objects a decisive significance has the action of metric singularity cut-off effect. In each of them the infalling masses have steadily filled whole inside of event horizon sphere and in due course have formed a thick shell. Thereat a concentration of particles by increasing has achieved the threshold value and afterwards the metric singularity

Table 4

THE PARAMETERS OF ACTIVE GALACTIC NUCLEI

Object	Type	Waveband of variability	$x_0(0)$	$x(0)$	$n(0)$ (cm^{-3})	$r(0)$ (cm)	$\rho(0)/\rho_0$	$P(0)/P_0$
1	2	3	4	5	6	7	8	9
NGC 4051	S1	X—ray/opt	6.83	13	3.104E+40	6.84E—04	9.49E+05	1.56E+08
NGC 5548	S1	ultraviolet	7	13	3.104E+43	6.84E—04	2.84E+07	4.70E+08
3C 371	BL LAC	opt	7.2	12.65	3.104E+43	6.84E—04	2.65E+07	4.50E+08
IZW 187	BL LAC	X—ray/opt	7.2	12.63	2.794E+43	6.84E—04	2.42E+07	4.27E+08
NGC 7469	S1	X—ray	8	18.9	3.104E+40	6.84E—04	3.92E+06	6.11E+08
MCG 8—11—11	S1	X—ray/opt	8	16	3.104E+44	6.84E—04	3.47E+08	2.33E+09
NGC 3227	S1	X—ray/opt	8.59	16	1.242E+49	6.84E—04	1.16E+14	3.05E+14
MkN 766	S1	opt	11	23	3.104E+43	6.84E—04	1.38E+08	1.44E+09
MkN 509	S1	X—ray	11	22.3	3.104E+43	6.84E—04	1.26E+08	1.34E+09
PkS 0521—36	BL LAC	opt	11	19.799	2.173E+43	6.84E—04	6.98E+07	9.37E+08
MkN 421	BL LAC	X—ray	11	19.5	3.104E+49	6.84E—04	4.77E+14	8.53E+14
Cen A	RG	X—ray	10.85	17	3.104E+57	2.74E—05	1.85E+25	4.11E+25
MkN 501	BL LAC	IR	16.24	24.1	3.104E+40	6.84E—04	9.96E+06	1.52E+09
NGC 7582	NELG/S2	X—ray	16.77	24	3.104E+40	6.84E—04	9.80E+06	1.49E+09
NGC 3516	S1	opt	17.95	24	3.104E+40	6.84E—04	9.80E+06	1.49E+09
106_8	S2	IR	18.53	24.1	3.104E+43	6.84E—04	1.59E+08	1.61E+09
[illegible]14	S1	X—ray	19.72	24	3.104E+40	6.84E—04	9.80E+06	1.49E+09
MkN 1 0	S1	opt	21.89	24	3.104E+43	6.84E—04	1.57E+08	1.59E+09
NGC 2110	NELG/S2	X—ray	25	24	3.104E+44	6.84E—04	8.82E+08	3.75E+09
4151	S1	X—ray	24.8	24	3.104E+43	6.84E—04	1.57E+08	1.59E+09
C6	NELG/S2	X—ray	25.6	24	3.104E+47	6.84E—04	1.57E+12	2.24E+12

Table 4 (Continued)

1	2	3	4	5	6	7	8	9
NGC 2992	NELG/S2	X—ray	27.05	24.7	3.104E+47	6.84E—04	1.63E+12	2.21E+12
NGC 3783	S1	X—ray/opt	38.85	27.7	2.793E+41	6.84E—04	2.76E+07	2.27E+09
MCG 5—23—16	NELG/S2	X—ray	39.67	27.7	3.104E+41	6.84E—04	2.85E+07	2.25E+09
NGC 526A	NELG/S2	X—ray	42.45	27.77	3.104E+43	6.84E—04	2.45E+08	2.27E+09
ApLibrae	BL LAC	opt	52	27.7	3.104E+43	6.84E—04	2.43E+08	2.26E+09
BL LAC	BL LAC	opt	77	29.2	3.104E+40	6.84E—04	2.18E+07	3.26E+09
NGC 1275	BL LAC	opt	99.32	31.23	3.104E+40	6.84E—04	2.72E+07	4.05E+09
3C 120	S1	X—ray	120	32	3.104E+41	6.84E—04	4.89E+07	3.79E+09
IIIZW2	S1	X—ray	125	31.1	3.104E+43	6.84E—04	3.49E+08	3.04E+09
MR 2251+11	QSO	opt	157	32.03	3.104E+43	6.84E—04	3.84E+08	3.28E+09
PkS 0736+01	QSO	opt	157	32.04	3.104E+43	6.84E—04	3.85E+08	3.29E+09
PkS 0548—30	BL LAC	opt	160	32.05	3.104E+41	6.84E—04	4.93E+07	3.81E+09
3C 390.3	S1	opt	160	32.05	3.104E+40	6.84E—04	3.01E+07	4.48E+09
PkS 1218+30	BL LAC	X—ray	200	32.04	3.104E+48	6.84E—04	4.09E+13	2.91E+13
LB 9743	QSO	X—ray	200	32.04	3.104E+45	6.84E—04	1.37E+10	2.17E+10
3C 334	QSO	opt	200.5	32.04	3.104E+45	6.84E—04	1.37E+10	2.17E+10
2S 0241+62	QSO.	X—ray	200.5	32.04	3.104E+45	6.84E—04	1.37E+10	2.17E+10
PkS 2208—13	QSO	opt	289	32.04	1.552E+44	6.84E—04	7.17E+09	1.41E+10
PHL 1657	QSO	opt	200	32.1	3.104E+40	6.84E—04	3.03E+07	4.50E+09
PkS 1510—89	QSO	opt	350	33.5	3.104E+45	6.84E—04	1.51E+10	2.19E+10
OJ 287	BL LAC	IR	398	33.5	3.104E+45	6.84E—04	1.51E+10	2.19E+10
3C 351	QSO	opt	1000	34.4	1.966E+40	2.74E—02	5.68E+07	5.16E+09
PkS 0420—01	QSO	opt	500	33.7	1.966E+40	2.74E—02	1.51E+10	2.34E+10

1	2	3	4	5
NAB 0137+01	QSO	opt	500	33.
OX 169	QSO	X—ray	498	33.
PkS 2155—30	BL LAC	X—ray	500	33.
CTA 102	QSO	opt	600	34.
3C 454.3	QSO	opt	600	34.
3C 345	QSO	opt	560	34
PkS 1355—41	QSO	opt	1000	34.
4C 29.45	QSO	opt	1000	34.
3C 273	QSO	X—ray	1000	34.
3C 446	QSO	opt	1000	34.
3C 263	QSO	opt	1000	34.
3C 66A	BL LAC	opt	1000	35
W10846+51	BL LAC	IR/opt	1069	34.
PkS 0537—44	QSO	opt	1070	34.
PkS 0735+17	BL LAC	IR	1500	34.
B2 1308+32	BL LAC	IR/opt	2000	35
AQ 0235+16	BL LAC	IR	2000	35

Table 4 (Continued)

	6	7	8	9
7	3.104E+44	6.84E−04	1.51E+10	2.34E+10
7	3.073E+44	6.84E−04	1.51E+10	2.19E+10
7	3.073E+44	6.84E−04	1.51E+10	2.19E+10
6	6.201E+42	6.84E−04	2.10E+08	3.86E+09
6	6.198E+42	6.84E−04	2.10E+08	3.86E+09
	3.104E+44	6.84E−04	2.17E+09	6.84E+09
4	1.552E+46	6.84E−04	1.09E+12	1.15E+12
4	1.986E+40	1.37E−02	5.68E+07	5.16E+09
4	1.964E+40	1.37E−02	5.68E+07	5.16E+09
4	1.964E+40	1.37E−02	5.68E+07	5.16E+09
4	1.963E+40	1.37E−02	5.68E+07	5.16E+09
	1.963E+40	1.37E−02	6.07E+07	5.50E+09
9	3.104E+43	1.37E−02	5.07E+08	4.13E+09
9	1.964E+40	5.47E−04	5.06E+08	4.13E+09
9	3.104E+45	1.37E−02	1.65E+10	2.24E+10
	9.023E+57	1.37E−05	1.59E+26	1.93E+25
	9.022E+57	1.37E−05	1.59E+26	1.92E+25

Table 5

THE INTEGRAL PARAMETERS OF ACTIVE GALACTIC NUCLEI

Object	$M/M_\odot$	R_n (km)	R_g (km)	DR (km)	N/N_0	$A1$	$A2$
1	2	3	4	5	6	7	8
NGC 4051	8.63E+02	749	2549	2.99E+08	10627	10.1	0.903
NGC 5548	1.26E+03	1063	3708	7.68E+10	17648	11.6	0.915
3C 371	1.39E+03	1172	4132	9.49E+10	20173	11.9	0.918
IZW 187	1.39E+03	1172	4133	1.22E+11	20161	11.9	0.917
NGC 7469	1.47E+03	1261	4333	8.42E+09	23667	13.1	0.926
MCG 8—11—11	1.88E+03	1572	5544	5.08E+10	31994	13.9	0.930
NGC 3227	2.60E+03	2140	7691	1.06E+10	49766	15.7	0.938
MkN 766	3.78E+03	3117	11157	1.76E+11	91947	19.9	0.951
MkN 509	3.87E+03	3184	11432	9.89E+10	94089	19.9	0.951
PkS 0521—36	4.29E+03	3475	12664	7.68E+10	103356	19.8	0.951
MkN 421	4.68E+03	3779	13813	2.49E+10	116831	20.6	0.952
Cen A	5.58E+03	4442	16472	2.17E+09	142849	21.2	0.954
MkN 501	9.90E+03	7842	29253	7.51E+10	349182	29.2	0.966
NGC 7582	1.08E+04	8535	31927	3.85E+10	393879	30.2	0.967
NGC 3516	1.28E+04	10032	37701	1.53E+11	499058	32.4	0.969
NGC 1068	1.47E+04	11504	43316	4.32E+09	616749	34.9	0.972
NGC 6814	1.68E+04	13096	49673	2.98E+07	724687	35.8	0.972
MkN 10	2.29E+04	17758	67715	2.60E+11	1144210	41.5	0.976
NGC 2110	2.98E+04	23049	88121	5.08E+10	1715708	47.9	0.979
NGC 4151	3.21E+04	24667	94800	7.01E+09	1819922	47.2	0.979
NGC 5506	3.51E+04	26955	103674	4.32E+09	2092089	49.7	0.980

Table 5 (Continued)

1	2	3	4	5	6	7	8
NGC 2992	3.83E+04	29448	113213	3.35E+10	2416887	52.6	0.981
NGC 3783	7.27E+04	55504	214831	2.54E+09	6394559	73.4	0.986
MCG 5—23—16	7.86E+04	59865	232217	2.99E+10	7063269	75.1	0.987
NGC 526A	8.80E+04	67088	259962	4.03E+10	8641666	82.1	0.988
ApLibrae	1.57E+05	118289	463109	2.66E+08	1.89E+07	100.7	0.990
BL LAC	4.33E+05	323756	1279508	3.06E+08	7.49E+07	145.3	0.993
NGC 1275	6.33E+05	473055	1870982	2.78E+10	1.42E+08	188.1	0.995
3C 120	7.52E+05	562622	2221571	2.99E+09	2.06E+08	229.9	0.996
IIIZW2	1.26E+06	937291	3721634	2.37E+09	3.65E+08	243.7	0.996
MR 2251+11	1.62E+06	1203372	4776189	3.94E+10	5.89E+08	306.1	0.997
PkS 0736+01	1.81E+06	1342709	5334794	2.17E+10	6.58E+08	306.2	0.997
PkS 0548—30	2.05E+06	1523113	6057538	5.19E+10	7.48E+08	306.7	0.997
3C 390.3	2.42E+06	1796565	7149711	7.34E+10	8.74E+08	303.6	0.997
PkS 1218+30	2.75E+06	2038073	8107134	9.03E+10	1.29E+09	394.9	0.998
LB 9743	3.21E+06	2378150	9465580	1.43E+07	1.49E+09	392.7	0.998
3C 334	3.59E+06	2665188	1.06E+07	1.64E+10	1.68E+09	393.8	0.998
2S 0241+62	3.59E+06	2665188	1.06E+07	4.96E+10	1.68E+09	393.8	0.998
PkS 2208—13	4.28E+06	3174646	1.27E+07	1.84E+10	2.09E+09	410.2	0.998
PHL 1657	5.20E+06	3853400	1.54E+07	2.17E+10	2.35E+09	379.6	0.997
PkS 1510—89	7.52E+06	5574628	2.22E+07	1.89E+10	6.14E+09	687.5	0.999
OJ 287	1.18E+07	8736422	3.49E+07	—	1.09E+10	781.7	0.999
3C 351	1.46E+07	1.08E+07	4.32E+07	1.93E+10	3.34E+10	1921.7	0.999
PkS 0420—01	1.46E+07	1.08E+07	4.32E+07	1.34E+10	3.34E+10	1921.7	0.999

Table 5 (Continued)

1	2	3	4	5	6	7	8
NAB 0137+01	2.08E+07	1.54E+07	6.13E+07	4.52E+10	2.42E+10	981.9	0.999
OX 169	2.36E+07	1.75E+07	6.97E+07	1.39E+09	2.74E+10	978.2	0.999
PkS 2155—30	2.47E+07	1.83E+07	7.29E+07	5.00E+09	2.88E+10	982	0.999
CTA 102	2.93E+07	2.17E+07	8.65E+07	1.27E+10	4.05E+10	1166.5	0.999
3C 454.3	2.93E+07	2.17E+07	8.65E+07	7.40E+07	4.05E+10	1166.5	0.999
3C 345	3.33E+07	2.46E+07	9.84E+07	3.51E+07	4.34E+10	1097.3	0.999
PkS 1355—41	4.00E+07	2.96E+07	1.18E+08	1.96E+10	9.36E+10	1969.1	0.999
4C 29.45	5.24E+07	3.87E+07	1.55E+08	1.48E+10	1.19E+11	1920.3	0.999
3C 273	6.25E+07	4.62E+07	1.85E+08	1.09E+10	1.43E+11	1920.4	0.999
3C 446	6.25E+07	4.62E+07	1.85E+08	7.18E+08	1.43E+11	1920.4	0.999
3C 263	6.62E+07	4.89E+07	4.89E+07	1.96E+08	1.51E+11	1920.7	0.999
3C 66A	7.37E+07	5.45E+07	2.18E+08	—	1.68E+11	1917.1	0.999
W10846+51	1.14E+08	8.45E+07	3.38E+08	1.77E+10	2.84E+11	2088.4	0.999
PkS 0537—44	1.32E+08	9.77E+07	3.90E+08	1.33E+10	3.28E+11	2088.4	0.999
PkS 0735+17	1.56E+08	1.15E+08	4.60E+08	1.76E+10	5.45E+11	2945.7	0.999
B2 1308+32	2.58E+08	1.90E+08	7.61E+08	—	1.22E+11	3981.6	0.999
A0 0235+16	2.91E+08	2.15E+08	8.61E+08	1.31E+10	1.38E+11	3981.7	0.999

cut-off effect has acted. As a matter of fact the event horizon sphere has vanished and the particles and light can already escape from the object to the outside wold. Just those very extreme conditions are presented in BL Lac objects—OJ 287, 3C 66A and B2 1308 + 32, the observed sizes of which almost are less than the sizes of corresponding spheres of event horizon in order of magnitude. This also may serve as a further strong indication that the presented here theory is preferable.

Tables 4, 5 present the whole set of basic integral characteristics of considered sources. Meanwhile this data cannot clear up the entire relations between all the characteristics. Therefore here also the results of some new calculations present which are represented by means, of e. g. figure 4, on which the radial profiles of density and pressure of the source Ap Librae is plotted.

7. *Discussion and conclusions.* A number of conclusions are drawn and the main features of our treatment are outlined below. The initial three sections of the present work have been dedicated to the general description of an alternative approach to the understanding of internal structure of highly compact stationary supermassive celestial bodies. In this connection the equations of equilibrium configurations of baryonic protomatter (ECBP) have been considered.

a) In the fourth section we have just discussed the question: to what results will the theory lead in a particular case of the absence of inner distortion of space-time continuum in the region of strong gravitational fields, which are typical for compact neutron stars? The answer is as follows. The possible maximum values of total masses of the equilibrium configurations of ideal degenerated neutron gas equal $M/M_{\odot} = 0.717 \div 0.74$, with corresponding radii $R = (8.5 \div 9\,8)$ km. Thus, the theory [8—10], which uses new conceptions of gravitational interaction [1] leads almost to the same results as well as the classical calculations of Oppenheimer and Volkoff [18] by means of Einstein's theory. That is a suggested gravitational theory and General Relativity are indiscernible up to the region of neutron stars.

The results of multiple numerical integrations are summarized in table 1 and are presented by means of corresponding diagrams.

b) In the fifth section the numerical integrations of the equations of ECBP already in the presence of the process of inner distortion of space-time continuum are carried out. Displayed under these conditions new phenomena directly relate to the global properties of a space-time continuum at small space-time intervals. That is why they hold irrespective of the choice of a concrete model of configuration. Due to it,

as the further calculations have proved, the modifications of models in a sense of change of the form of state equation cannot lead to the perceptible corrections. This enables to carry out the calculations for a most simple case of equilibrium one-component configurations of degenerated ideal neutron gas in the presence of one-dimensional space-like inner distortion of space-time continuum. It has been shown that in the central parts of the considered configurations, where the distances bet-

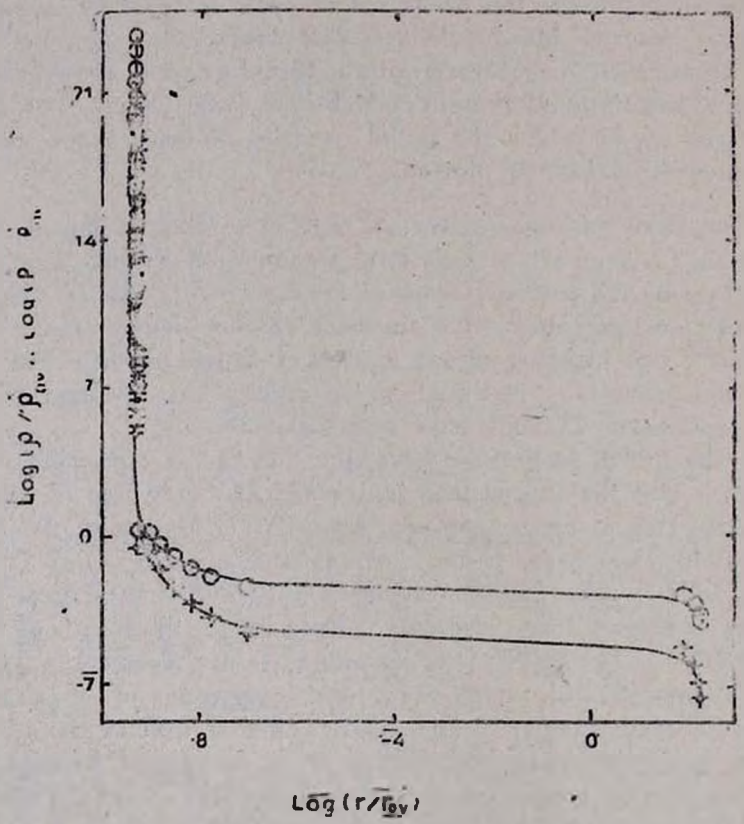

Fig. 4. The radial profiles of the density and pressure of the source Ap Librae ($P_{ov} = 6.469 \times 10^{36}$ (erg cm^{-3}), $\rho_{ov} = 7.194 \times 10^{15}$ (g. cm^{-3}), $r_{ov} = 13.68$ (km).
$\circ$ — Log (ρ/ρ_{ov}), $+$ — Log (P/P_{ov}).

ween the particles are less than the threshold value ($\leqslant 0.4$ Fermi) of the proceeding of process of inner distortion of space and time, the stable stationary supermassive cores of neutron protomatter are formed. Alongside with some other new processes, it is important to note that

in particular, each neutron undergoes to the phase transition. The shift of mass at rest, energy-momentum spectra of particle and due to it the shift of energy of gas as a whole upwards along the energy scale took place. Because of the presence of process of inner distortion of space and time, in the central region of superdense core of neutron proto-matter the pressure rises proportional to the sharp increase of gravitational forces of compression. This one counteracts to the catastrophic compression of the central region. Hence the stable equilibrium remains valid in the outward layers of the central core too, even up to limit of masses much greater than Solar mass. According to calculations, these stable cores have been wholly found within their spheres of event horizon. Just because of it they can be observed only in the presence of accreting matter in their immediate vicinities. Connected to it only the configurations consisting of mentioned above stable stationary supermassive central cores surrounded by accretion disks are considered. The fundamental difference from standard black hole accretion models is the fact that central cores are in stable equilibrium state with certain radial distributions of density and pressure, and with a number of integral characteristics such as the masses M, M_1, M_0, radius R_n, total number of baryons N, the gravitational packing coefficients and so on. Versus these parameters of central cores such configurations present concrete models of AGNs.

The numerous integrations enable one to establish the significant effect of metric singularity cut-off, the whole point of which briefly comes to the following. In those cases when central value of concentration of neutrons is less than $n(0)^{-1/3} = 0.4$ Fermi, the process of inner distortion of space-time continuum is absent from the very outset. Then a singularity of metric develops. Drawing near-by to the sphere of event horizon the gravitational forces of compression and concentration of neutrons sharply increase. The latter at last achieves the threshold value and a mechanism counteracting to the further development of singularity is engaged afterwards. That is, under such conditions the field of inner distortion is switched on, the singularity of metric disappears and the inverse process of decrease of concentration as well as the gravitational forces begins. Hence a singularity ceases to signify and the metric singularity cut-off process is presented.

By means of multiple numerical integrations one is able to reveal another fact of a great importance, which is the presence within the outlined theory the rigorous restriction on the upper limit of possible values of total masses of considered configurations. This limit has to be equaled $M \leqslant 3.5 \cdot 10^8 M_\odot$. The equilibrium configurations with the

masses greater than this value cannot exist just because of strong violation of subsidiary condition of sewing of gravitational potential. The esults of numerical integrations are presented in tables 2 and 3. To be more complete and for clearing up the whole set of relations between different integral characteristics one fills a want with corresponding diagrams for configurations characterized by concrete central values of potentials of the field of gravitation and inner distortion of space and time.

c) According to the results of the previous section we were convinced in the correctness of the statement that the further modifications of the considered models in the sense of the change of the form of state equation to the other one of real baryonic gas could not actually lead to perceptible corrections. This fact enables one to proceed to the direct modelling of concrete AGNs in sixth section, the whole point of which is reduced to the following. Based on observational data, for the very first, one defined a total mass M of concrete object. Afterwards one solves the inverse problem. That is by means of reiterated integrations of the equations of ECNP one determined those required central values of concentration of particles and potential of field of inner distortion, for which the calculated total mass of configuration has been exactly equaled to the same value M. It is clear that after the integrations one also obtains the whole set of basic integral characteristics of the considered objects.

The results of those multiple integrations for the 61 sources are presented in tables 4, 5. As an example, these data are also appended by new calculations, the results of which are represented by corresponding diagram including the radial profiles of density and pressure of the Ap Librae source.

At last one should emphasize the important fact of the existence of exotic stationary objects such as the—OJ 287, 3C 66A and B^2 1308 + 32 in Nature. This fact clearly shows the fundamental difference between the outlined approach to the understanding of internal structure of the considered celestial bodies and the standard accretion models. Actually, in spite of the auxiliary assumption of asymmetric emission geometry, nevertheless for these objects the observed timescales for flux variations are inconsistent with the contemporary black hole accretion models. The case in quite different within the scope of our approach. It seemed that a decisive significance for those objects has the action of metric singularity cut-off effect. In each of them the infalling masses have steadily filled a whole inside of event horizon sphere and in due course have formed a thick shell around the central core. Ther ea.

a concentration of particles by increasing has achieved to the threshold value after which the mentioned above effect has been acted. As a matter of fact the event horizon sphere has vanished and the particles and light are enabled to escape already from the objects to the outside wold. Just those very extreme conditions are presented in BL Lac objects—OJ 287, 3C 66A and B2 1308 + 32, the observed sizes of which almost in order of magnitude are less than the sizes of corresponding spheres of event horizon. This may serve as a further indication that the worked out here theory is preferable against standard models.

Acknowledgements: I am grateful for discussions and collaboration with many astrophysicists, especially academician V. A. Ambartsumian for useful comments on various issues treated in the present paper. I thank also H. A. Grigorian, A. V. Sarkissian and particularly A. A. Beglarian for unselfish investment of time and for providing with technical assistance. Among others, I am hugely obliged to A. M. Vardanian for his steady encouragement and support during the preparation of this work.

Byurakan astrophysical
observatory

О ВНУТРЕННЕМ СТРОЕНИИ СВЕРХМАССИВНЫХ КОМПАКТНЫХ НЕБЕСНЫХ ТЕЛ

Г. Т. ТЕР-КАЗАРЯН

Предложен новый подход к задаче внутреннего строения сверх компактных стационарных массивных небесных тел, принципиально отличающийся от современных стандартных аккреционных моделей черных дыр. Рассмотрены уравнения равновесных конфигураций барионного протовещества (РКБП). В частном случае вырожденного идеального нейтронного газа при отсутствии процесса внутреннего искажения пространства—времени показано, что предложенная автором теория приводит к тем же результатам, полученные Оппенгеймером и Волковым по теории гравитации Эйнштейна. Проведено численное интегрирование уравнений РКБП в наиболее простом случае вырожденного идеального нейтронного газа при одномерном пространственноподобном чисто внутреннем искажении пространства—времени. Показано, что в центральных областях рассматриваемых конфигураций образуются сверхмасивные устойчивые стационарные ядра. В качестве моделей активных галактических ядер (АГЯ) рассмотрены именно конфигурации, состоящие из этих ядер, окруженных аккреционными дисками. Принципиальным различем от стандартных аккреционных моделей черных дыр является то, что центральные ядра находятся в состоянии устойчивого равновесия с оп-

ределенными радиальными распределениями плотности и давления, а также с некоторыми интегральными характеристиками. Выявлен важный эффект обрезания сингулярности метрики, из-за действия которого сингулярность метрики перестает быть существенным. Путем многократных интегрирований установлен также другой важный факт о наличии в теории жесткого ограничения сверху на возможные значения полных масс рассматриваемых конфитураций, который равен $M \leqslant 3.5 \cdot 10^8 M_\odot$ В последнем разделе проведено моделирование конкретных объектов АГЯ (61 источников), суть которого сводится к решению обратной задачи. Результаты всех вычислений представлены в таблицах, а также рисунками, изображающими некоторые зависимости интегральных характеристик. Наконец, следует отметить факт существования экзотических стационарных объектов, какими являются лацертиды OJ 287, 3C 66A и B2 1308+32, наблюдательные данные о переменности излучения которых не согласуются с предсказаниями стандартных моделей. Совсем иначе обстоит дело в рамках предложенной теории. По-видимому для них решающее значение имеет действие эффекта обрезания сингулярности метрики, из-за действия которого наблюдаемые размеры этих объектов почти на порядок меньше размеров соответствующих сфер горизонта событий. Это может указывать на то, что предложенная теория предпочтительнее по сравнению со стандартными моделями.

REFERENCES

1. *G. T. Ter-Kazarian*, Communications of Byurakan Obs., 62, 1989.
2. *Witta*, Comments Astrophys., 9, 261, 1982.
3. *M. I. Rees*, Ann. Astron. Astrophys., 22, 471, 1984.
4. *D. L. Band, M. A. Malkan*, IAU Symposium, 134, 253, 1989.
5. *C. D. Impey*, "BL Lac Objects: Ten Years After" Conference, Como, Italy, 1988
6. *L. Bassani, A. I. Dean, S. Sembey*, Astron. Astrophys, 125, 52, 1983.
7. *L. Bassani, A. I. Dean*, Prepr. Univ. Southampton, Dept. Phys., Southampton, S09 5NH, U. K., 1983.
8. *G. T. Ter-Kazarian*, Astrophysica, SSSR, 31, No 2, 345, 1989.
9. *G. T. Ter-Kazarian*, Astrophysica SSSR, 33, No 1, 143, 1990.
10. *G. T. Ter-Kazarian*, Doklady Akad. Nauk., SSSR, 305, No 1, 97, 1989.
11. *C. D. Impey, G. Neugebauer*, Astron. J., 95, No 2, 307, 1988.
12. *S. L. Shapiro, S. A. Teukolsky*, Black Holes, White Dwarfs and Neutron Stars Cornell Univ., Ithaca, New York, 1983.
13. *B. K. Harrison, K. S. Thorne, M. Wakano* and *I. A. Wheeler*, Gravitation Theory and Gravitational Collapse, Univ. Chicago Press, Chicago, Illinois, 1965.
14. *G. Baym, H. A. Bethe* and *C. I. Pethick*, Nucl. Phys., A 175, 225, 1971.
15. *H. Satz*, Statistical Mechanics of Quarks and Hadrons, North-Holland Publ Company, Amsterdam, 1981.
16. *I. L. Elliot, S. L. Shapiro*, Astrophys. J., 192, 13, 1974.
17. *M. A. Abramovicz, L. Nobili*, Nature, 300, 506, 1982.
18. *I. R. Oppenheimer, G. M. Volkoff*, Phys. Rev., 55, 374, 1939.